Ionic transport features in concrete composites containing various shaped aggregates:

Liu, Qing-feng; Feng, Gan-lin; Xia, Jin; Yang, Jian; Li, Long-yuan

DOI:
10.1016/j.compstruct.2017.03.088

Document Version
Peer reviewed version

Citation for published version (Harvard):
Liu, Q, Feng, G, Xia, J, Yang, J & Li, L 2017, 'Ionic transport features in concrete composites containing various shaped aggregates: a numerical study', *Composite Structures*. https://doi.org/10.1016/j.compstruct.2017.03.088

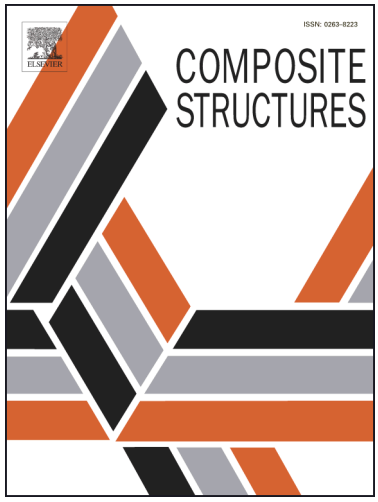

Ionic transport features in concrete composites containing various shaped inner structures: a numerical study

Qing-feng Liu, Gan-lin Feng, Jin Xia, Jian Yang, Long-yuan Li

PII: S0263-8223(17)30169-1
DOI: http://dx.doi.org/10.1016/j.compstruct.2017.03.088
Reference: COST 8409

To appear in: *Composite Structures*

Received Date: 18 January 2017
Revised Date: 16 March 2017
Accepted Date: 25 March 2017

Please cite this article as: Liu, Q-f., Feng, G-l., Xia, J., Yang, J., Li, L-y., Ionic transport features in concrete composites containing various shaped inner structures: a numerical study, *Composite Structures* (2017), doi: http://dx.doi.org/10.1016/j.compstruct.2017.03.088

Ionic transport features in concrete composites containing various shaped inner structures: a numerical study

Qing-feng Liu[a,b], Gan-lin Feng[c], Jin Xia[d], Jian Yang[a,e*] and Long-yuan Li[c]

a- State Key Laboratory of Ocean Engineering, School of Naval Architecture, Ocean & Civil Engineering, Shanghai Jiao Tong University, Shanghai, China

b- Collaborative Innovation Center for Advanced Ship and Deep-Sea Exploration (CISSE), Shanghai, China

c-School of Marine Science and Engineering, University of Plymouth, UK

d-Institute of Structural Engineering, Zhejiang University, Hangzhou, PR China

e-School of Civil Engineering, University of Birmingham, UK

Abstract

The service life of concrete-based infrastructure and buildings is seriously shortened due to the chloride-induced durability problems. In order to clarify the transport mechanism associated with the response of inclusion structures, this paper presents a numerical study on the influence caused by morphology and heterogeneity of individual phases, in which the concrete is treated as a three-phase composite including mortar, aggregates and interfacial transition zone (ITZ). A series of meso-scale numerical models with different shapes and volume fractions of aggregates are developed for examining the effects of aggregates on ionic migration. Unlike in most of the existing published research *work* in this area, a multi-component ionic transport theory which takes ionic interactions into consideration has been utilised in this study. By coupling mass conservation and Poisson's equations, the time-spatial concentration distribution results for individual ionic species are obtained. Other important factors such as the externally applied electric field, concrete heterogeneity, ionic binding and ITZ are also considered and examined in this study. Through this relatively thorough numerical analysis, some important features about the effect of aggregate shape based on multi-species modelling, which have previously not been properly investigated, are highlighted.

Keywords: durability; numerical modelling; concrete composites; inner structures of concrete; aggregate shape; chloride migration; heterogeneity; multi-phase; multi-species; ionic interaction; binding

*) *Corresponding author:*

Email: liuqf@sjtu.edu.cn (Q.-F. Liu), j.yang.1@sjtu.edu.cn (J. Yang)

1. Introduction

Concrete is the most widely used man-made material in modern construction industry. However, the service life of concrete-based infrastructure and buildings has been seriously shortened due to the durability problems, especially the corrosion of reinforcement caused by the penetration of chloride ions. Once the chloride concentration around the reinforcing steel reaches a threshold value, depassivation of the reinforcement will occur [1],[2]. To this end, it is important to clarify the transport mechanism associated with changes in ionic concentration in concrete, and how individual phases in concrete composites behave during chlorides penetration.

During the last few decades, a number of studies have been produced around the theme of assessment of ionic transport in concrete by using traditional methods, including analytical models [3]-[10] and experimental techniques [11]-[23]. Concrete is a composite material consisting of meso- and micro-structural organisations, which has a complicated heterogeneous nature. Unfortunately, most of the previous analytical studies are only capable of tackling one dimensional transport problems in a single-phase medium and are generally suitable for cement or mortar matrices, but not for concrete. Experimental studies have the advantage of providing credible and valuable data on transport properties of concrete; however, they are weak in clarifying the individual effects of different factors, as well as usually being time-consuming and expensive.

It seems that none of these earlier experimental or analytical methods is suitable for evaluating the influence of individual components on chloride transport in concrete. To deal with this, from the mechanics point of view, if the properties of each individual material involved in the concrete are known then the properties of the concrete composite should be predictable. For this concern, *advanced numerical concrete models*, which are originally

developed for structural stress analysis [24],[25], have recently been utilized to investigate the ionic transport properties of concrete, treating it as a multi-phase composite material [26]-[42]. By using these multi-phase computational models, it can be easy to clarify and quantify the influence of the different component parts of concrete, i.e. coarse/fine aggregate inclusion, mortar/cement and interfacial transition zones (ITZs), which could not be achieved with one dimensional (1-D) analytical models. However, most of the existing modelling work assumes that the shape of an aggregate particle is circular or spherical. This rough simplification may cause simulation results to be inaccurate. More recently, meso-structures of concrete with several aggregate shapes have been established to explore the effect of aggregate shape on the durability properties of concrete. As a typical example, Larrard et al. [44] numerically generated 3-D, 2-phase samples with and without steel bars to study the effects of the aggregate shape on drying and atmospheric carbonation. It was found that, regarding macroscopic indicators, the influence of the coarse aggregate shapes appears negligible when compared to the effect of their volume fractions. Li et al [45] established 3-D meso-scale models to investigate the effective permeability during steady state flow, and claimed that the tortuosity effect is more pronounced when different aggregate shapes are employed. *Abyaneh et al. [46] numerically explored the effect of aggregate size, shape and volume fraction on the capillary absorption. They solved the non-linear, non-steady state Fick's equation in a 3-D mesoscale model and found the shape of aggregate particles may have a significant effect on the water penetration profile and sorptivity.* Using chloride diffusivity as a durability indicator, Zheng et al. [47] applied a 2-D, 3-phase model using lattice method to investigate the effect of aggregate shape on chloride diffusion through concrete, in which the aggregate particles are assumed to be elliptical. They concluded that the chloride diffusivity in concrete decreases with an increase in the aspect ratio of elliptical aggregate particles. Abyaneh et al. [48] conducted a series of numerical simulations with a 3-

D *finite difference* model to study the effect of the shape of various spheroidal aggregates (i.e. spherical, tri-axial ellipsoidal, prolate spheroidal and oblate spheroidal). The results showed that the diffusivity decreased significantly when spherical aggregate particles were replaced by ellipsoidal aggregate particles, particularly for higher aggregate fractions and aspect ratios.

Most of transport models described above focus on the diffusion mechanism and employ Fick's law to describe the steady-state chloride diffusion in concrete with spheroidal aggregates. The ionic transport behaviour in saturated electrolyte solution is classified into both diffusion and migration, particularly for cases where an externally applied electric field is involved, such as in the rapid chloride permeability/migration test (RCPT/RCM) [21]-[23], and the electrochemical chloride removal (ECR) treatment [49]. The former is one of the most widely used test methods in durability testing; whereas the latter has recently become a popular rehabilitation method due to both its cost and efficiency. It is clearly essential for the numerical models to extend the ionic diffusion to a more complicated migration dominated process. In recent years, great efforts have been made on this issue [50]-[68]. However, the presence of an external electric field, and coupling between different species leads the transport equations to a highly nonlinear form. In order to achieve convergent solutions, most existing numerical simulations regarding migration only adopt a 1-D model or 2-D model, but incorporate a number of simplifications (e.g. circular aggregates).

The above literature review shows that the influence of inner structures morphology, i.e., various shaped aggregates on ionic transport in a multiple ionic electro-migration process within mortar or concrete has not been investigated in the existing models. In this paper, a numerical study is presented to simulate the chloride migration process by treating the concrete as a three-phase composite including mortar, ITZs and aggregates with various shapes and volume fractions. A series of meso-scale models are developed for a theoretical

investigation. The previous studies on the effect of aggregate shape [47],[48] did not discuss or show the details of chloride transport in concrete, such as the time-dependent concentration distribution and penetration depth (which are the key information for predicting the depassivation process or chloride diffusivity), and they modelled concrete with only spheroidal shaped inclusions. The study presented in this paper examines both spheroidal and polygonal aggregates, and also provides time-spatial distribution results for the four ionic species involved (K^+, Na^+, Cl^-, OH^-) by solving coupled mass conservation and Poisson's equations. Other important factors such as the externally applied electric field, concrete heterogeneity, ionic binding and the ITZs are also considered and examined in this study. Through this thorough numerical analysis based on multi-phase and multi-species modelling, some important features about the effect of aggregate shape, which have not previously been properly investigated, are highlighted.

2. Theoretical background

In order to discuss the ionic transport features in heterogeneous concrete subjected to an external electric field, more attention should be devoted to the definitions of driving forces, ionic binding, time-dependent concentration and electrical potential per unit of medium.

Fick's law is not adequate to describe the ionic transport other than the diffusion process. When a transport process includes various driving forces such as concentration gradient, electric field, pressure flow and chemical activity, the flux of ionic species can be presented by the extended Nernst-Planck equation as follows,

$$\mathbf{J}_k = -D_k \nabla C_k - \frac{z_k F}{RT} D_k C_k \nabla \Phi + C_k u_k - \frac{C_k}{\gamma_k} \nabla \gamma_k \tag{1}$$

where $\mathbf{J}_k$ and C_k are the flux and the concentration of the k-th species, respectively, D_k is the diffusion coefficient, u_k is the advective velocity, γ_k is the chemical activity coefficient, z_k is the charge number, F = 9.648×10^4 Cmol^{-1} is the Faraday constant, R = 8.314 J mol^{-1}K^{-1} is the ideal gas constant, T = 298 K is the absolute temperature, and Φ is the electrostatic potential. For the RCM test, as the pore solution is fully saturated with diluted solution and there are no pressure differences, the terms of convection and chemical activity can be ignored. Hence, the extended Nernst-Planck equation can be simplified to a diffusion-migration form, as follows:

$$\mathbf{J}_k = -D_k \nabla C_k - \frac{z_k F}{RT} D_k C_k \nabla \Phi \tag{2}$$

To quantitatively describe the time-spatial distribution of ionic concentrations, each ionic species involved in the electrolyte solution is also subjected to the mass conservation equations as described in Eq. (3),

$$\frac{\partial C_k}{\partial t} = -\nabla \cdot \mathbf{J}_k \tag{3}$$

where t is time. As the effect of the aggregate is involved in this study, the concrete considered here is modelled as a composite structure consisting of aggregate-, cement paste- and ITZ-phases at mesoscopic level. The cement paste phase and ITZ phase are treated as two different porous materials; different microstructure properties are applied in the numerical simulation to show their different transport properties. Thus the governing equations for ionic transport in this study *should be rewritten and taken* influences of the microstructure properties of the porous materials into account. In this study, porosity and tortuosity of the pore structure are considered to *represent* the microstructure effect. Adsorption and desorption of ions [69] at the pore walls while ions transport in the pore

structures are also considered. Normally the porosity and tortuosity effects are considered by adjusting the diffusion coefficient, but in this study these two parameters are considered by using the ionic transport equations in porous media. Adsorption and desorption are considered using *existing* ionic binding models. Finally Eq. (3) should be modified as follows:

$$\frac{\partial(\varphi C_k)}{\partial t} + \frac{\partial[(1-\varphi)S_k]}{\partial t} = -\varphi\nabla\cdot\mathbf{J}_k \tag{4}$$

where φ is the porosity and S_k is the concentration of bound ions. Three different methods (linear, Langmuir or Freundlich isotherm [70]) can be used to approximate the ratio between the bound and free chloride ions and the binding is nearly independent of the ionic transport rate. To enhance numerical stability, a simple linear isotherm [71] is used here:

$$\frac{(1-\varphi)}{\varphi} S_k = \lambda_k C_k \tag{5}$$

where $\lambda_k > 0$ is a dimensionless fitting constant for the k-th species. Substituting Eqs. (2) and (5) into Eq. (4) yields:

$$(1+\lambda)\frac{\partial C_k}{\partial t} = \nabla(D_k\nabla C_k) + \nabla\left[\left(\frac{z_k D_k F}{RT}\right)C_k\nabla\Phi\right] \tag{6}$$

During the ionic migration process, the electrostatic potential, Φ, in Eq. (6) is governed not only by the externally applied electric field, but also by the internal concentration imbalance between different species caused by different flow rate. The electrostatic potential should be decided by Gauss's law [72] as the following form of Poisson's equation,

$$\nabla^2\Phi = -\frac{F}{\varepsilon_0\varepsilon_r}\sum_{k=1}^{N} z_k C_k \tag{7}$$

where ε_o = 8.854×10^{-12} CV^{-1}m^{-1} is the permittivity of vacuum, ε_r = 78.3 is the relative permittivity of water at 298 K, and N is the total number of species involved in the simulation. Most of the existing work on multi-species transport is based on the assumption of electro-neutrality condition ($\sum_{k=1}^{N} z_k C_k = 0$) replacing Eq. (7) and thus $\nabla^2 \Phi = 0$, which means that the electrostatic potential, Φ, in Eq. (6) is only determined by the externally applied electric field. Though this assumption can reduce the computational difficulty, the ionic electro-coupling between different species cannot be realised, *which can lead to questionable results.* Literatures also indicate that the numerical models with consideration of interactions between multiple ionic species controlled by Poisson's equation, which is the more correct relationship between the electrostatic potential and the charge density, can provide more accurate results than those considering only one ionic species, or those considering multi-species in the pore solution but using the assumption of the electro-neutrality condition [51]-[55]. However, Poisson's equation brings huge difficulties in achieving convergent solutions and for now only the 1-D or 2-D simulation result for multi-species transport is available. N, this study will solve Eqs. (6) and (7) with given initial and boundary conditions to obtain the distribution profiles of electrostatic potential Φ and the concentration profiles of individual ionic species, at any place and any time in the solution domain.

3. Modelling

The concrete specimen modelled in this study is considered as a composite material with three phases, consisting of cement mortar matrix, coarse aggregates and ITZs. For simplification, in most of the existing multi-phase concrete models [26]-[43] including the authors' previous *works* [55], [64]-[67], the shape of the coarse aggregate was assumed to be

circular or spherical. In reality, the shape of coarse aggregates is not spherical in most cases. One of the 2-D multi-phase concrete models, with a sample size of 50×50 mm, is shown in Fig.1. The volume fraction of aggregate V_{agg} is 0.5 in this model. The circles represent the impermeable aggregates with radii ranging from 1.5 mm to 10 mm *with Fuller aggregate gradation.* The locations of the aggregates were randomly determined using a MATLAB program. *Regarding the statistical effects, at a certain volume fraction of aggregate, the diffusivity of a 2-D concrete performs a decent reproducibility due to the use of the same aggregate gradation.* The ITZs are considered as thin shell layers outside each aggregate particle, and the thickness of the ITZ layers in the model is assumed to be 40 μm *due to numerical difficulties in mesh size (the ITZ thickness is usually supposed to be 20-50 μm in normal concrete [74],[75]).* The remaining part of the model represents the cement mortar matrix. As well as using the aggregate volume fraction of 0.5, this study also conducted simulations with different concrete geometries and volume fractions (ranging from 0.1-0.5) of various shaped aggregates but these are not displayed here.

In order to further study the effect caused by different aggregate shapes and volume fractions, a set of newly developed 2-D models with various shapes and volume fractions of coarse aggregates are used in this study. Fig. 2 shows the models with the same volume fraction of aggregate (V_{agg} = 0.5) but different aggregate shapes, which are elliptical, triangular, rectangular, and mixed shapes. The various shaped ITZs wrapped around the aggregate particles are shown in the zoomed-in figure on the right-hand side of Fig.2, and are highlighted in blue. The finite element meshes are also shown in Fig.2, which shows that only the cement mortar phase and ITZs are meshed during modelling. The coarse aggregate particles are assumed to be impermeable *to save the simulation time. Note that due to the issue of Peclet number [55] and tiny scale of ITZs, the element size need to be finely meshed*

to achieve convergent solutions. Denser meshes bring more accurate result but much more time for computing. In this study, a minimum element size of 6.25 μm has been chosen to balance between the accuracy and computation time. It is also noticeable from Fig.2 that elliptical, triangular, and rectangular type aggregates are almost uniformly distributed within their respective concrete geometries, whereas the aggregates in the mixed shape model are less uniformly distributed. An elaborate examination of the model geometries including mixed shape aggregate particles shows that smaller sized particles gather more in the region near the cathode (from x=0m to x=0.025m), whereas the larger sized particles gather more in the region near the anode (from x=0.025m to x=0.05m). This mixed shape model has been intentionally developed in this way to investigate the influence of tortuosity *and to show the effect of aggregate size to some extent*, which is explained and discussed later.

The models described above are then employed to simulate the RCM test [21]-[23], in which concrete specimens are placed between two compartments and an external DC voltage of 24V is applied between the two surfaces of the specimen. The compartment with the cathode inserted is filled with 0.52 mole/l NaCl solution and the compartment with the anode inserted is filled with 0.30 mole/l NaOH solution. The whole RCM test set-up is illustrated in Fig.3. Four ionic species (i.e. K^+, Na^+, Cl^-, OH^-) are analysed in the simulations. Other ionic species (e.g. Ca^{2+} and SO_4^{2-}) are not considered in the present simulations owing to their low concentrations in the concrete specimen. The ionic transport parameters employed in this numerical study are listed in Table 1, and the initial and boundary conditions are shown in Table 2 *[73]. For the conditions shown in Table 2 and the aforementioned meshing settings, it takes almost one day to achieve one convergent result on a PC of 2.5 GHz quad-core processors and 16G RAM, depending on the number of degree of freedom which is, for example, 0.98 million in the model shown in Fig.2 (southeast).*

4. Results and Discussion

With given initial and boundary conditions, the five field variables (i.e. electrostatic potential and concentrations of K^+, Na^+, Cl^-, and OH^-) in the simulated 3-phase concrete specimens can be numerically calculated by solving the mass conservation equation and the Poisson equation. The 3-D plots shown in Figs. 4 and 5 provide a good visualized view of the evolution of the variables, in which the two plane coordinates represent the position of the 2-D concrete model with 50% volume fraction of various shaped aggregates, and the vertical coordinate is the results of the variable. Each frame of an individual variable represents one unique moment during the first 4 hours of the simulated RCM test. It can be seen from Fig. 4 that when using Poisson's equation to control the multi-species ionic transport, electrostatic potential increases from $\Phi = 0$ at the cathode to $\Phi = 24$ V at the anode, but this relationship is clearly not linear. It is interesting to note from the 3-D plot that the electrostatic potential curve varies from a convex shape after the first hour to a concave shape after the fourth hour. This means that initially migration speed of ionic species is higher in the region near the cathode, but over time the zone with higher ionic migration speed moves to the anode. The results show that migration speed of chloride ions is not be constant and varies not only in time but also in space.

In terms of the four ionic concentrations, because the penetration of chloride ions and the effect of aggregate shape on it are of particular interest, only the distribution profiles of chloride concentration are shown in the form of a 3-D plot in Fig.5. With the same aggregate volume fraction, the evolution of ionic transport in the models with elliptical, triangular, rectangular and mixed shape aggregate particles is very similar to that in the circular aggregate model *which has been validated against experimental data [65]*. The negatively charged chloride ions are driven steadily from the cathode towards the anode in the migration

process along the x-axis, which can be observed through the visible ‘migration wave front’. It can also be seen from the figures that the migration wave fronts of chloride ions are split into sections by the impermeable aggregate particles, which makes the wave front act like a ‘waterfall’. Generally, the moving velocity of the wave front ‘waterfall’ is almost the same along the y-axis, apart from in the model using triangular shaped aggregate, as shown in Fig.5c. This phenomenon can be explained by the effect of tortuosity. The sharp angles of the triangular shape significantly increase the length of the flow path and create a lot of local corner pockets in the electrolyte solution, which slows down the transport of ions in corresponding areas.

For a more quantitative study, Figs. 6-9 employ traditional 2-D plots to show comparisons of the concentration profiles of four ionic species with five different aggregate shapes. Considering the results of the different ionic species, as a result of the nonlinear electrostatic potential gradient, the ionic species coupling can be observed by the similar migration speed of the same charged ions. Considering the results of different aggregate shapes, it is clear that there is only a tiny difference in the migration velocities between the models with the “obtuse” shapes (i.e. circular, elliptical and rectangular), which gives a similar tortuosity. In contrast, from the overall point of view, the migration velocities with the model using triangular aggregate are the lowest among the five different models, which is mainly due to the higher tortuosity.

More interesting features can be found upon closer examination of the curves of the mixed shape model. As mentioned above, the different shaped aggregates are deliberately arranged to be less uniformly distributed (the small sized particles gather more near the cathode side, and the larger ones gather more near the anode side). The tortuosity of this model is correspondingly less uniform (with higher tortuosity in the area near the cathode, and lower

tortuosity in the area near the anode). As a consequence, the speed of the migration wave front of the negatively charged ions (Cl^- and OH^-) in the mixed shape model is much slower than that in the models using circular, elliptical and rectangular aggregates in the section from x=0m to x=0.025m, but it is a little higher than that in the triangular shape model. In the section from x=0.025m to x=0.05m, close to the anode, the speed of the migration wave front of the negatively charged ions in the mixed shape model is much higher than that in the triangular shape model, and is nearly the same as the results in the obtuse shape models. Governed by the electrochemical multi-species coupling, the results for the positively charged ions (K^+ and Na^+) show exactly the opposite trend. The phenomenon discussed above clearly shows how the tortuosity *(caused by aggregate size)* regionally affects ionic transport in concrete.

The above findings show that under the condition of identical volume fraction but with different aggregate distribution scenarios, the effect of aggregate shape has a significant impact on ionic migration. The aggregate particles lead to higher tortuosity of concrete in the triangular shape model, but in the circular, elliptical and rectangular shape models the aggregate shape has little impact, leading to lower tortuosity of concrete in these cases. *Interestingly, this phenomenon is similar to what happened in Abyaneh's model [48]. The triangle aggregate herein acts like the tri-axial ellipsoidal and oblate spheroidal aggregates of higher aspect ratios. This shows that the tortuosity effect can play significant roles in both 2-D migration and 3-D diffusion models.* To further demonstrate this finding, more examples are provided here of different aggregate particle shapes with various volume fractions (ranging from 0% to 50%). Figs. 10, 11 and 12 show the comparisons of different shapes under the aggregate volume fractions of 30%, 40% and 45%, respectively. As expected, the earlier observations from the simulations under the condition of identical volume fraction of aggregate can be seen in simulations with different volume fractions of aggregate. Figs.10-12

again show that the migration velocities of chloride ions are approximately identical when comparing the models with various shapes, apart from in the model using triangular aggregates, which leads to a significantly higher tortuosity. Moreover, by referring to the results under the condition of different volume fractions of aggregates (i.e. 50%, 45%, 40% and 30%), it can be found that the effect of aggregate shape increases with the aggregate volume fraction. Note that the aggregates of mixed shapes in the models with 30%, 40% and 45% fractions are randomly distributed. Therefore, the special phenomenon caused by the tortuosity difference which occurs in Figs. 6-9 disappears in Figs. 10-12.

Figure 13 shows the distribution profiles of Cl^- concentration comparing three different aggregate volume fractions. As expected, the smaller the aggregate volume fraction is, the quicker the chloride ions travel. This is likely to be due to the tortuosity effect. As the aggregate volume fraction increases, tortuosity gets higher, thus the ionic transport slows down. However, due to the presence of the ITZ phase (in which the ions travel much faster than in bulk mortar), the discrepancy in the results between different volume fractions is not so remarkable. It can be seen that the higher aggregate volume fraction is also accompanied by a higher ITZ volume fraction. It can also be seen by careful examination of the influence of aggregate shape, as shown in the concentration profiles (Fig. 8 and Fig. 13), that the impact of aggregate shape appears to be more significant than the effect of their volume fractions. For example, the variation in velocity between circular and triangular shapes is greater than that between 30% and 50% volume fractions; the variation in velocity between the other three shapes is also close to that between the 40% and 50% volume fractions. These findings clearly emphasise the significance of exploring the aggregate shape effect on ionic electro-migration in multi-phase models.

5. Conclusions

This paper presents a *numerical* investigation into the transport features of chloride migration in concrete composite based on a 3-phase model, which considers various shapes (both spheroidal and polygon) and volume fractions of aggregates. The model also considers ionic interactions, ionic binding, the non-steady state process and external voltage, to simulate a multi-component transport process during RCM testing. From this study the following conclusions can be drawn:

1) The proposed multi-phase, multi-component transport model provides a promising tool for demonstrating the transport features, such as how ionic concentration changes in concrete and how individual phases behave while chlorides penetrate the concrete composites. In this model, the electrostatic potential gradient, which is also the dominant source of ionic transport, is no longer linear, but varies not only in time but also in space.

2) The 2-D concentration distribution *profiles* show that the irregular tortuosity caused by various shaped aggregates will markedly influence the length of the flow paths of ions as well as the ionic diffusivity. In addition, the distribution scenario of coarse aggregates will also have an impact on ionic transport.

3) Under the condition of identical volume fraction of aggregates, the effect of aggregate shape has *significant* impact on the ionic migration rate when the aggregate shapes have higher tortuosity, whereas it has little impact when the aggregate shapes have lower tortuosity.

4) Under the condition of different volume fractions of aggregates, the effect of aggregate shape increases with the aggregate volume fraction.

5) The comparison between the effects of shape and volume fraction suggests that, in addition to the volume fraction of aggregates, the aggregate morphology is also an important factor to consider in modelling the concrete composites.

Acknowledgements

The work was supported by the Natural Science Foundation of China (51508324), the Shanghai Pujiang Program, China (15PJ1403800) and the Shanghai Chenguang Program, China (16CG06).

References

[1] Z.P. Bazant. Physical model for steel corrosion in concrete sea structures—theory. Journal of the Structural Division 105 (1979) 1155–1166.
[2] F. Yan, Z. Lin. Bond durability assessment and long-term degradation prediction for GFRP bars to fiber-reinforced concrete under saline solutions. Composite Structures 161 (2017) 393–406.
[3] A. Atkinson, A. K. Nickerson. The diffusion of ions through water-saturated cement. Journal of Materials Science 19 (1984) 3068–3078.
[4] D.W. Hobbs. Aggregate influence on chloride ion diffusion into concrete. Cement and Concrete Research 29 (1999) 1995–1998.
[5] E. J. Garboczi. Permeability, diffusivity, and microstructural parameters: a critical review. Cement and Concrete Research 20 (4) (1990) 591–601.
[6] J. V. Brakel, P. M. Heertjes. Analysis of diffusion in macroporous media in terms of porosity, a tortuosity and a constrictivity factor. International Journal of Heat & Mass Transfer 17 (9) (1974) 1093–1103.
[7] E.J. Garboczi, D.P. Bentz. Analytical formulas for interfacial transition zone properties. Advanced Cement Based Materials 6(3-4) (1997) 99–108.
[8] K. Xu, J.F. Daian, D. Quenard. Multiscale structures to describe porous media part II: transport properties and application to test materials. Transport in Porous Media 26 (3) (1997) 319-338.
[9] Y. Xi, Z.P. Bazant. Modeling chloride penetration in saturated concrete. Journal of Materials in Civil Engineering 11 (1999) 58–65.
[10] H.O. Byung, Y.J. Seung. Prediction of diffusivity of concrete based on simple analytical equations. Cement and Concrete Research 34(3) (2004) 463–480.
[11] AASHTO T 259, Standard Method of Test for Resistance of Concrete to Chloride Ion Penetration, American Association of States Highway and Transportation Officials, Washington, 2003.
[12] ASTM C1543, Standard Test Method for Determining the Penetration of Chloride Ion into Concrete by Ponding, ASTM International, West Conshohocken, PA, 2010.

[13] S. Amidi, J. Wang. Deterioration of the FRP-to-concrete interface subject to moisture ingress: Effects of conditioning methods and silane treatment. Composite Structures 153 (2016) 380–391.
[14] D. Whiting. Rapid measurement of the chloride permeability of concrete. Public Roads 45 (3) (1981) 101–112.
[15] H. Li, H. Xiao, X. Guan, Z. Wang, L. Yu. Chloride diffusion in concrete containing nano-TiO2 under coupled effect of scouring. Composites Part B 56 (2014) 698–704.
[16] AASHTO T 277, Standard Method of Test for Rapid Determination of the Chloride Permeability of Concrete, American Association of States Highway and Transportation Officials, Washington, 1983.
[17] ASTM C 1202, Standard Test Method for Electrical Indication of Concrete's Ability to Resist Chloride Ion Penetration, American Society for Testing and Materials, Philadelphia, 1994.
[18] J.P. Won, Y.N. Yoon, B.T. Hong, T.J. Choi, S.J. Lee. Durability characteristics of nano-GFRP composite reinforcing bars for concrete structures in moist and alkaline environments. Composite Structures 94 (2012) 1236–1242.
[19] H.L. Su, J. Yang, T.C. Ling, G. Ghataora, S. Dirar. Properties of concrete prepared with waste tyre rubber particles of uniform and varying sizes. Journal of Cleaner Production 91 (2015) 288–296.
[20] B.M. Miyandehi, A. Feizbakhsh, M.A. Yazdi, Q.F. Liu, J. Yang, P. Alipour. Performance and properties of mortar mixed with nano-CuO and rice husk ash. Cement & Concrete Composites 74 (2016) 225–235.
[21] L. Tang, L.O. Nilsson. Rapid determination of the chloride diffusivity in concrete by applying an electric field. ACI Materials Journal. 89 (1) (1993) 49–53.
[22] NT-Build 492. Nordtest Method: Concrete, Mortar and Cement-Based Repair Materials: Chloride Migration Coefficient from Non-Steady-State Migration Experiments. (1999).
[23] AASHTO TP 64-03, Standard Method of Test for Prediction of Chloride Penetration in Hydraulic Cement Concrete by the Rapid Migration Procedure, American Association of State Highway and Transportation Officials, Washington, 2003.
[24] F. Bernard, S. Kamali-Bernard. Predicting the evolution of mechanical and diffusivity properties of cement pastes and mortars for various hydration degrees – A numerical simulation investigation. Computational Materials Science 61 (2012) 106–115.
[25] M.G. Alberti, A. Enfedaque, J.C. G alvez, E. Reyes. Numerical modelling of the fracture of polyolefin fibre reinforced concrete by using a cohesive fracture approach. Composites Part B 111 (2017) 200–210.
[26] D.P. Bentz, E.J. Garboczi. Percolation of phases in a three-dimensional cement paste microstructural model. Cement and Concrete Research 21(2-3) (1991) 325–344.
[27] B. Bourdette, E. Ringot, J.P. Ollivier. Modeling of the transition zone porosity. Cement and Concrete Research 25(4) (1995) 741–751.
[28] E.J. Garboczi, D.P. Bentz. Multiscale analytical/numerical theory of the diffusivity of concrete. Advanced Cement Based Materials 8(2) (1998) 77–88.
[29] C.C. Yang, S.H. Weng. A three-phase model for predicting the effective chloride migration coefficient of ITZ in cement-based materials. Magazine of Concrete Research 65(3) (2013) 193–201.
[30] S. Caré. Influence of aggregates on chloride diffusion coefficient into mortar. Cement and Concrete Research 33(7) (2003) 1021–1028.
[31] S. Caré, E. Hervé. Application of a n-phase model to the diffusion coefficient of chloride in mortar. Transport Porous Media 56(2) (2004) 119–135.
[32] Y.W. Zeng. Modeling of chloride diffusion in hetero-structured concretes by finite element method. Cement & Concrete Composites 29 (2007) 559–565.

[33] J.J. Zheng, H.S. Wong, N.R. Buenfeld. Assessing the influence of ITZ on the steady-state chloride diffusivity of concrete using a numerical model. Cement and Concrete Research 39 (2009) 805–813.
[34] G. Sun, Y. Zhang, W. Sun, Z. Liu, C. Wang. Multi-scale prediction of the effective chloride diffusion coefficient of concrete. Construction and Building Materials 25 (2011) 3820–3831.
[35] J. Xiao, J. Ying, L. Shen. FEM simulation of chloride diffusion in modeled recycled aggregate concrete. Construction and Building Materials 29 (2012) 12–23.
[36] J.Y. Jiang, G.W. Sun, C.H. Wang. Numerical calculation on the porosity distribution and diffusion coefficient of interfacial transition zone in cement-based composite materials. Construction and Building Materials 39 (2013) 134–138.
[37] J. Ying, J. Xiao, L. Shen, M.A. Bradford. Five-phase composite sphere model for chloride diffusivity prediction of recycled aggregate concrete. Magazine of Concrete Research 65(9) (2013) 573–588.
[38] L.Y. Li, J. Xia, S.S. Lin. A multi-phase model for predicting the effective diffusion coefficient of chlorides in concrete. Construction and Building Materials 26 (1) (2012) 295–301.
[39] J.J. Zheng, X.Z. Zhou, Y.W. Wu, X.Y. Jin. A numerical method for the chloride diffusivity in concrete with aggregate shape effect. Construction and Building Materials 31 (2012) 151–156.
[40] A. Caporale, L. Feo, R. Luciano. Damage mechanics of cement concrete modeled as a four-phase composite. Composites Part B 65 (2014) 124–130.
[41] L. Wang, J. Bao, T. Ueda. Prediction of mass transport in cracked-unsaturated concrete by mesoscale lattice model. Ocean Engineering 127 (2016) 144–157.
[42] Q.F. Liu, L.Y. Li, D. Easterbrook, D. Li. Prediction of chloride diffusion coefficients in concrete using meso-scale multi-phase transport models. Magazine of Concrete Research 69 (2017) 134–144.
[43] S.D. Abyaneh, H.S. Wong, N.R. Buenfeld. Simulating the effect of microcracks on the diffusivity and permeability of concrete using a three-dimensional model. Computational Materials Science 119 (2016) 130–143.
[44] T. de Larrard, B. Bary, E. Adamc, F. Kloss. Influence of aggregate shapes on drying and carbonation phenomena in 3D concrete numerical samples. Computational Materials Science 72 (2013) 1–14.
[45] X. Li, Y. Xu, S. Chen. Computational homogenization of effective permeability in three-phase mesoscale concrete. Construction and Building Materials 121 (2016) 100–111.
[46] S.D. Abyaneh, H.S. Wong, N.R. Buenfeld. Computational investigation of capillary absorption in concrete using a three-dimensional mesoscale approach. Computational Materials Science 87 (2014) 54–64.
[47] J.J. Zheng, X.Z. Zhou, Y.W. Wu, X.Y. Jin. A numerical method for the chloride diffusivity in concrete with aggregate shape effect. Construction and Building Materials 31 (2012) 151–156.
[48] S.D. Abyaneh, H.S. Wong, N.R. Buenfeld. Modelling the diffusivity of mortar and concrete using a three-dimensional mesostructure with several aggregate shapes. Computational Materials Science 78 (2013) 63–73.
[49] D.R. Lankard, J.E. Slatter, W.A. Holden, D.E. Niest. Neutralization of chloride in concrete, FHWA Report No. FHWA-RD-76-6, Battelle Columbus Laboratories, (1975).
[50] G.A. Narsillo, R. Li, P. Pivonka, D.W. Smith. Comparative study of methods used to estimate ionic diffusion coefficients using migration tests. Cement and Concrete Research 37 (2007) 1152–1163.
[51] B. Johannesson, K. Yamada, L.O. Nilsson, Y. Hosokawa. Multi-species ionic diffusion in

concrete with account to interaction between ions in the pore solution and the cement hydrates. Materials and Structures 40 (2007) 651–665.
[52] E. Samson, J. Marchand. Modeling the transport of ions in unsaturated cement-based materials. Computers & Structures 85 (2007) 1740–1756.
[53] K. Krabbenhoft, J. Krabbenhoft. Application of the poisson-nernst-planck equations to the migration test. Cement and Concrete Research 38 (2008) 77–88.
[54] J. Xia, L.Y. Li. Numerical simulation of ionic transport in cement paste under the action of externally applied electric field. Construction and Building Materials 39 (2013) 51–59.
[55] Q.F. Liu, L.Y. Li, D. Easterbrook, J. Yang. Multi-phase modelling of ionic transport in concrete when subjected to an externally applied electric field. Engineering Structures 42 (2012) 201–213.
[56] M.M. Jensen, B. Johannesson, M.R. Geiker. Framework for reactive mass transport: Phase change modeling of concrete by a coupled mass transport and chemical equilibrium model. Computational Materials Science 92 (2014) 213–223.
[57] L.Y. Li, C.L. Page. Modelling and simulation of chloride extraction from concrete by using electrochemical method. Computational Materials Science 9 (1998) 303–308.
[58] F. Frizon, S. Lorente, J.P. Ollivier, P. Thouvenot. Transport model for the nuclear decontamination of cementitious materials. Computational Materials Science 27 (2003) 507–516.
[59] O. Truc, J.P. Ollivier, L.O. Nilsson. Numerical simulation of multi-species transport through saturated concrete during a migration test--MSDIFF code. Cement and Concrete Research 30 (2000) 1581–1592.
[60] Y. Wang, L.Y. Li, C.L. Page. A two-dimensional model of electrochemical chloride removal from concrete. Computational Materials Science 20 (2001) 196–212.
[61] A. Toumi, R. Francois, O. Alvarado. Experimental and numerical study of electrochemical chloride removal from brick and concrete specimens. Cement and Concrete Research 37 (2007) 54–62.
[62] Y. Liu, X. Shi. Ionic transport in cementitious materials under an externally applied electric field: Finite element modeling. Construction and Building Materials 27 (2012) 450–460.
[63] B. Šavija, M. Luković, E. Schlangen. Lattice modeling of rapid chloride migration in concrete. Cement and Concrete Research 61–62 (2014) 49–63.
[64] Q.F. Liu, J. Xia, D. Easterbrook, J. Yang, L.Y. Li. Three-phase modeling of electrochemical chloride removal from corroded steel-reinforced concrete. Construction and Building Materials 70 (2014) 410–427.
[65] Q.F. Liu, D. Easterbrook, J. Yang, L.Y. Li. A three-phase, multi-component ionic transport model for simulation of chloride penetration in concrete. Engineering Structures 86 (2015) 122–133.
[66] Q.F. Liu, J. Yang, J. Xia, D. Easterbrook, L.Y. Li, X.Y. Lu. A numerical study on chloride migration in cracked concrete using multi-component ionic transport models. Computational Materials Science 99 (2015) 396–416.
[67] G.L. Feng, L.Y. Li, B. Kim, Q.F. Liu. Multiphase modelling of ionic transport in cementitious materials with surface charges. Computational Materials Science 111 (2016) 339–349.
[68] L.Y. Li, D. Easterbrook, J. Xia, W.L. Jin. Numerical simulation of chloride penetration in concrete in rapid chloride migration tests. Cement & Concrete Composites 63 (2015) 113–121.
[69] J. Geng, D. Easterbrook, Q.F. Liu, L.Y. Li. Effect of carbonation on release of bound chlorides in chloride-contaminated concrete. Magazine of Concrete Research 68 (2016) 353–363.

[70] L. Tang, L.O. Nilsson. Chloride binding capacity and binding isotherms of OPC pastes and mortars. Cement and Concrete Research 23 (1993) 247–253.
[71] D.P. Bentz, E.J. Garboczi, Y. Lu, N. Martys, A.R. Sakulich, W.J. Weiss. Modeling of the influence of transverse cracking on chloride penetration into concrete. Cement and Concrete Composites 38 (2013) 65–74.
[72] B. Johannesson. Comparison between the Gauss' law method and the zero current method to calculate multi-species ionic diffusion in saturated uncharged porous materials. Computers and Geotechnics 37 (2010) 667–677.
[73] C.C. Yang, S.W. Cho. The relationship between chloride migration rate for concrete and electrical current in steady state using the accelerated chloride migration test. Materials and Structures 37(2004) 456–63.
[74] S. Diamond, J.D. Huang. The ITZ in concrete – a different view based on image analysis and SEM observations. Cement and Concrete Composites 23 (2001) 179-188.
[75] J.M. Gao, C.X. Qian, H.F. Liu, B. Wang, L. Li. ITZ microstructure of concrete containing GGBS. Cement and Concrete Research 35 (2005) 1299-1304.

Table 1. Ionic transport properties in different phases

Field variables	Potassium	Sodium	Chloride	Hydroxide
Charge number	1	1	-1	-1
Diffusion coefficient in aggregates, D_A	0	0	0	0
Diffusion coefficient in bulk mortar, $D_{B,}$ $\times 10^{-10}$ m^2/s	1.96	1.33	2.03	5.26
Diffusion coefficient in ITZs, D_I $\times 10^{-10}$ m^2/s	9.80	6.65	10.15	26.30

Table 2. Initial and boundary conditions of individual species

Field variables		Potassium	Sodium	Chloride	Hydroxide	Electrostatic potential
Concentration boundary conditions, mole/m^3	x = 0	0	520	520	0	0
	x = L	0	300	0	300	24 V
Flux boundary conditions	y = 0	J = 0	J = 0	J = 0	J = 0	əΦ/əy=0
	y = L	J = 0	J = 0	J = 0	J = 0	əΦ/əy=0
Initial conditions, mole/m^3	t = 0	200	100	0	300	0

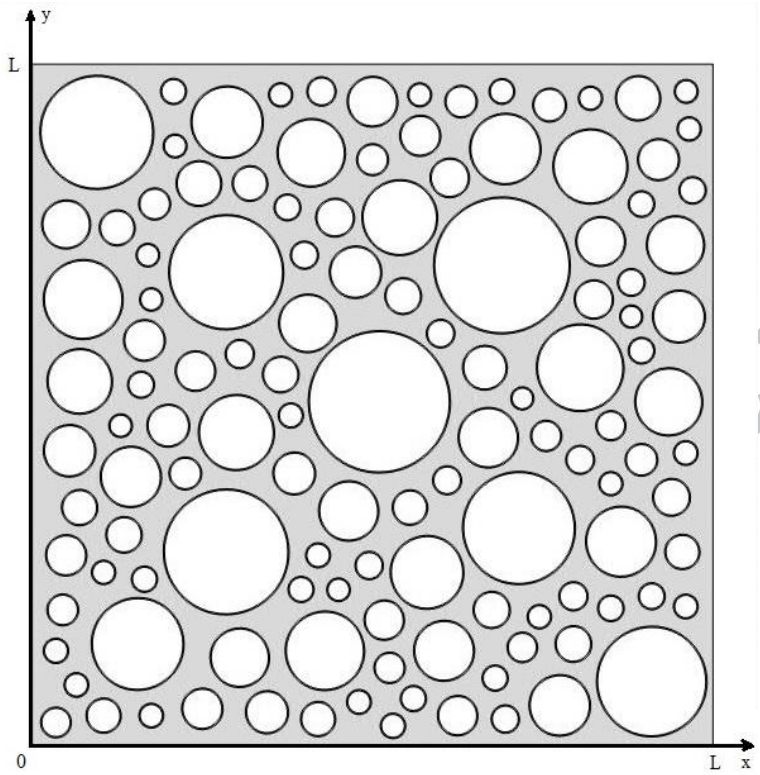

Figure 1. Geometry sample of 2D multi-phase concrete model: section of concrete, V_{agg} = 0.5.

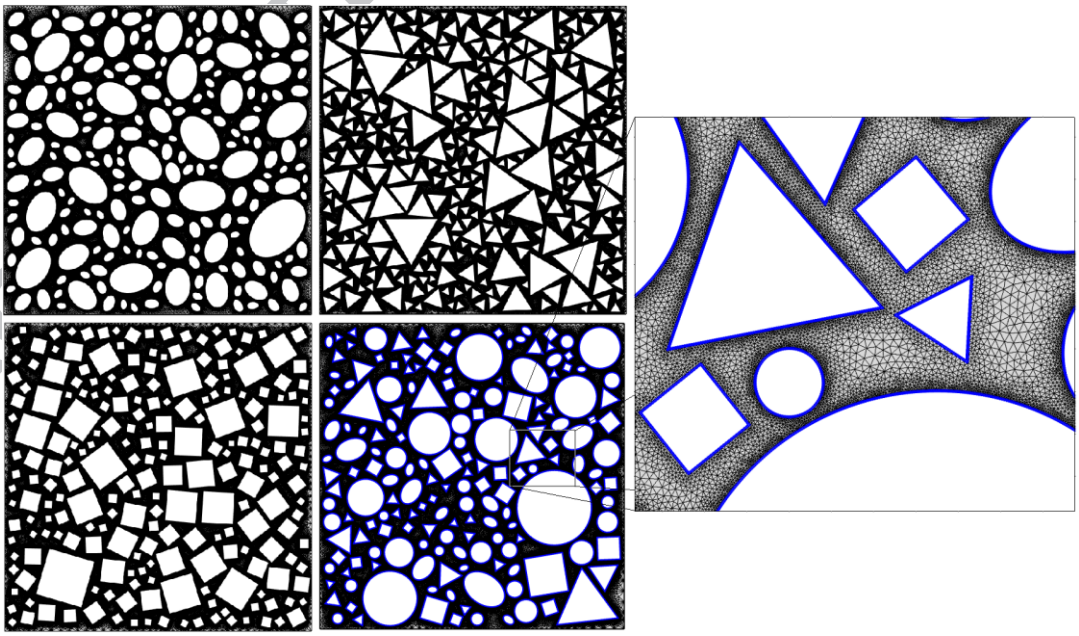

Figure 2. Finite element mesh of geometries with various shaped aggregates, V_{agg} = 0.5.

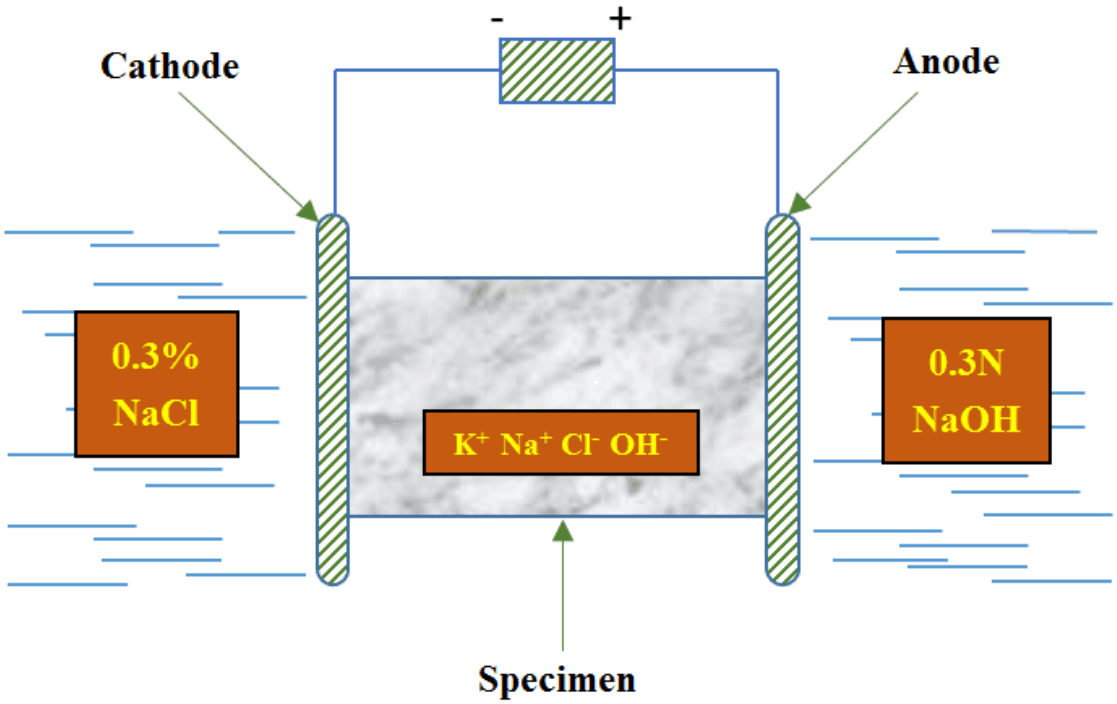

Figure 3. Schematic representation of 2-D plain concrete specimen in a RCM test.

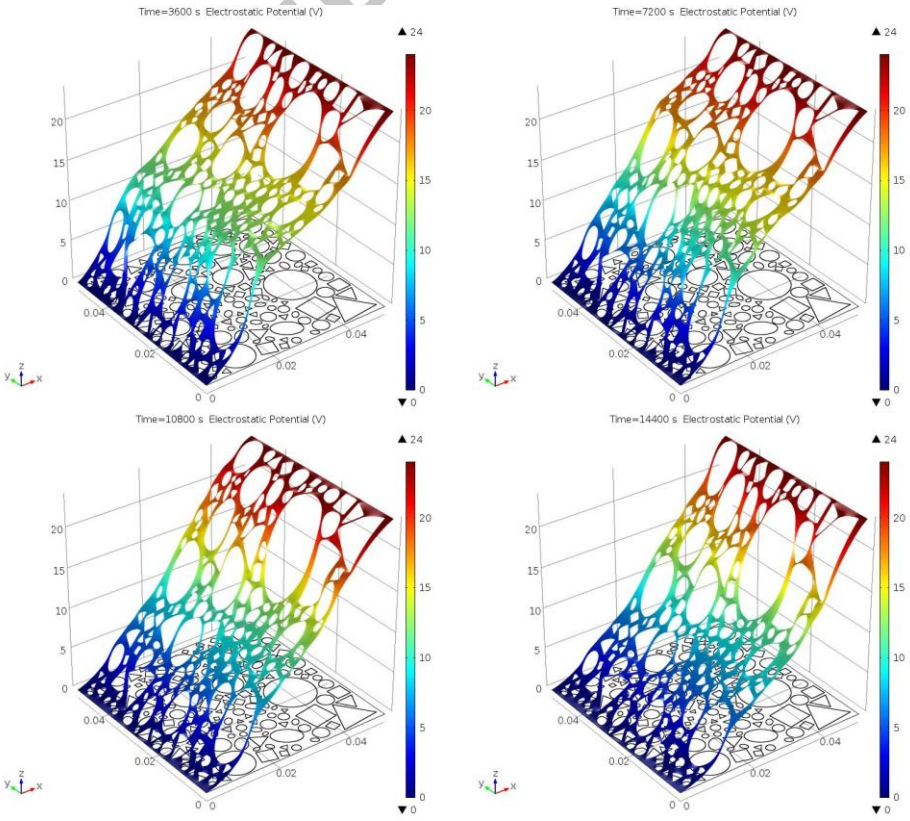

Figure 4. Electrostatic potential distribution profiles (for aggregates with mixed shapes).

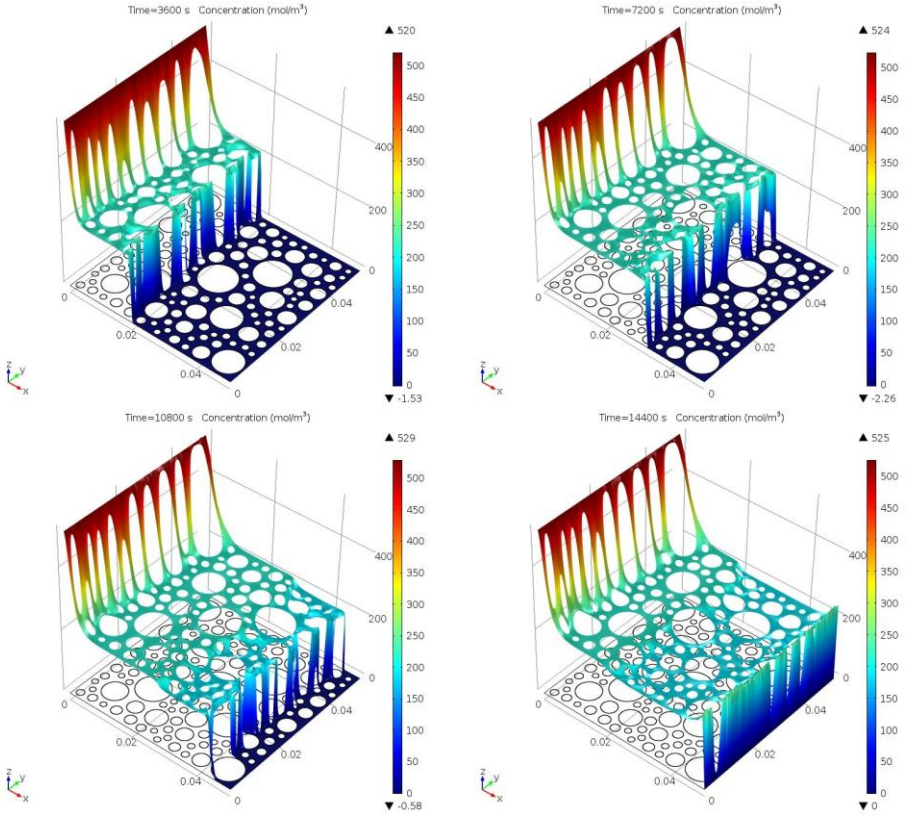

Figure 5a. Concentration distribution profiles of chloride ions (for aggregates with a circular shape).

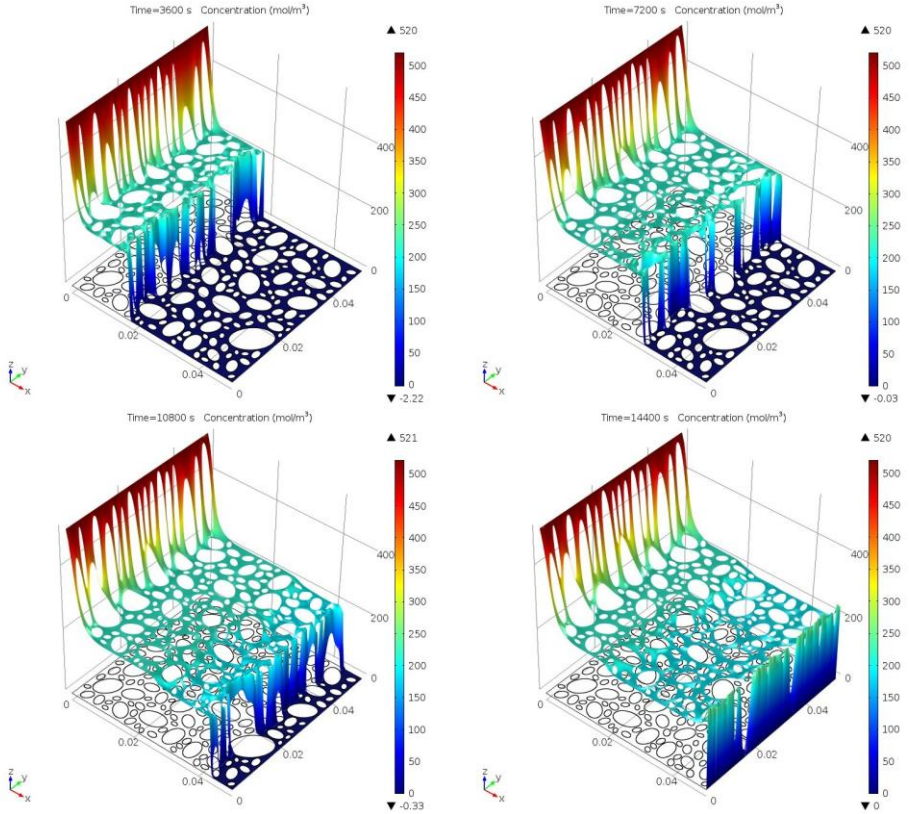

Figure 5b. Concentration distribution profiles of chloride ions (for aggregates with an elliptical shape).

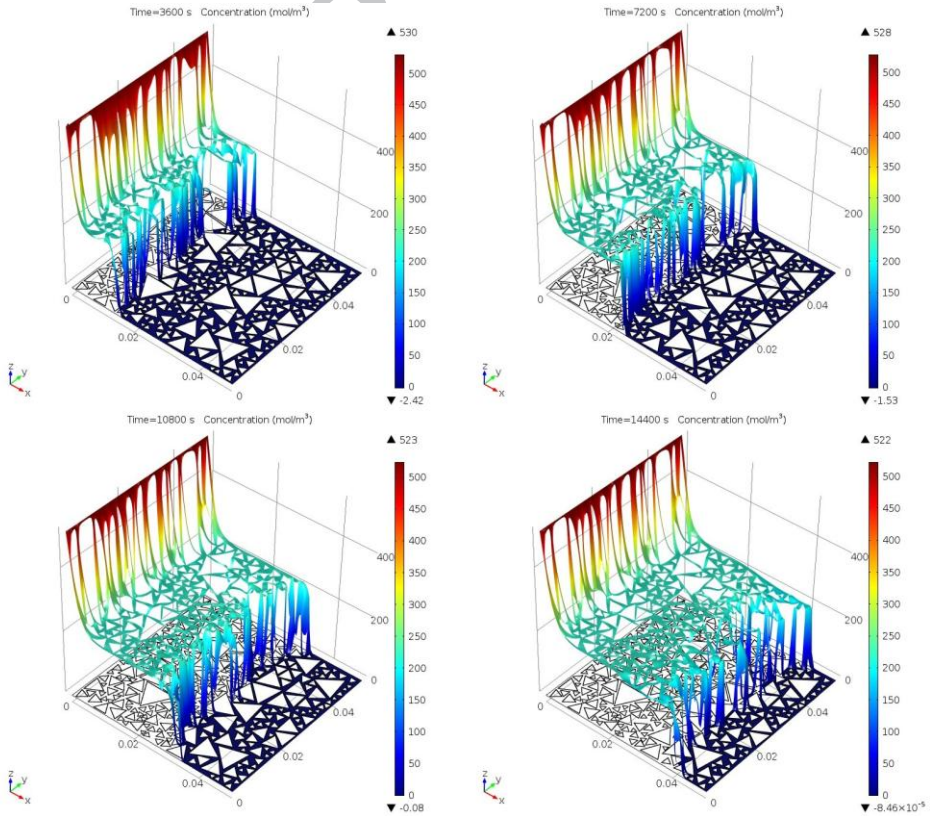

Figure 5c. Concentration distribution profiles of chloride ions (for aggregates with a triangular shape).

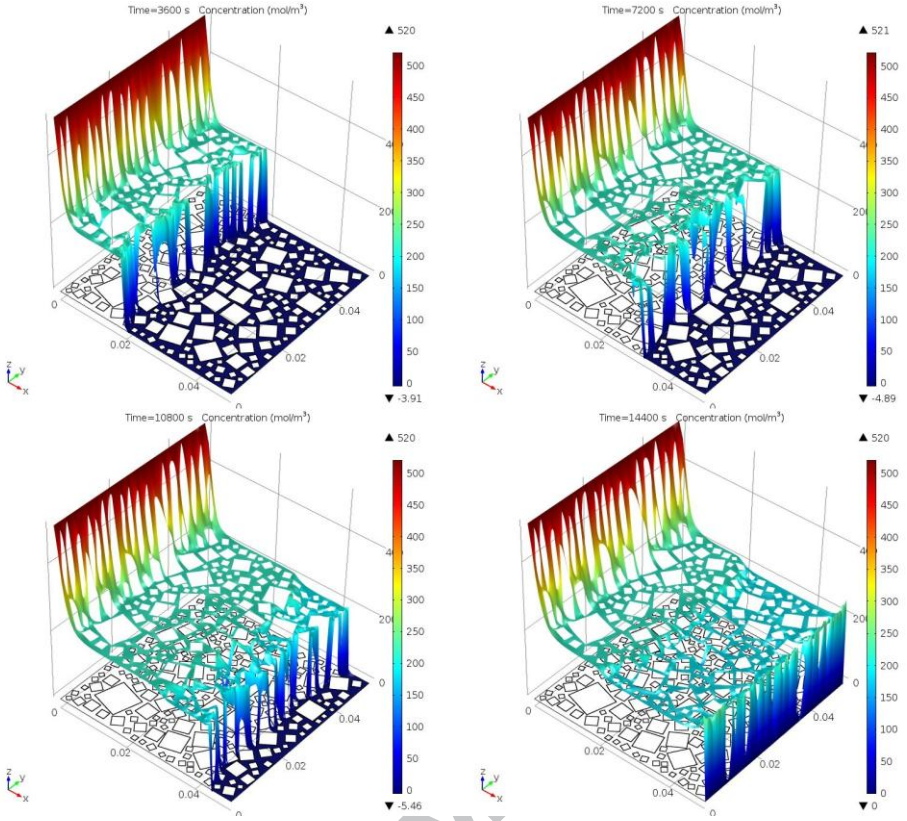

Figure 5d. Concentration distribution profiles of chloride ions (for aggregates with a rectangular shape).

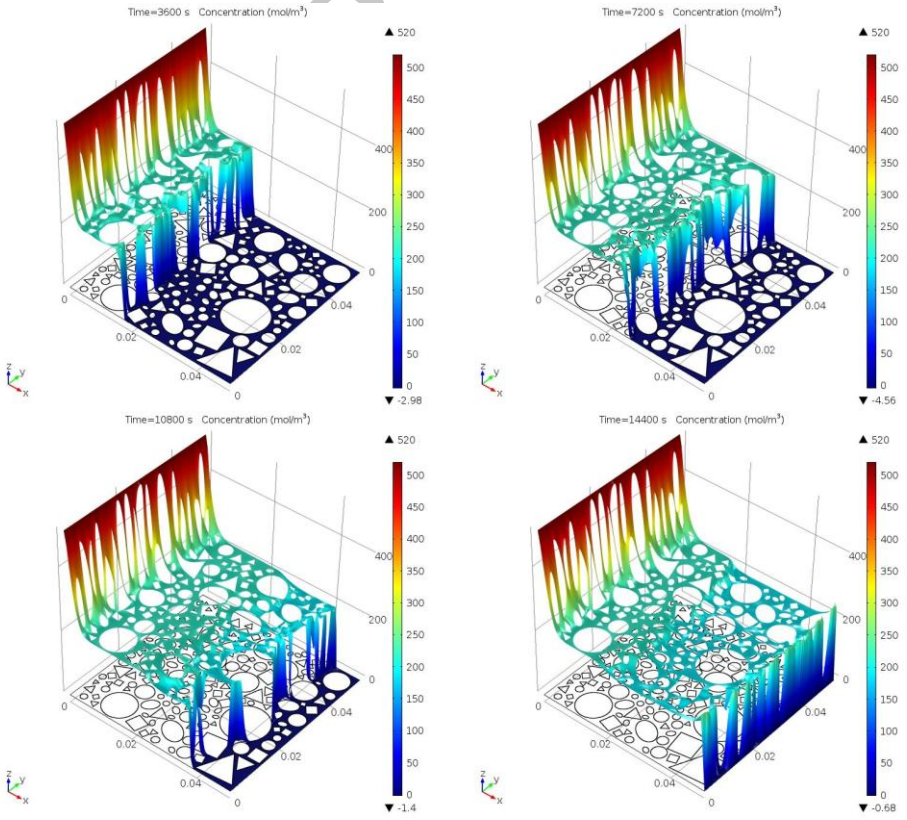

Figure 5e. Concentration distribution profiles of chloride ions (for aggregates with mixed shapes).

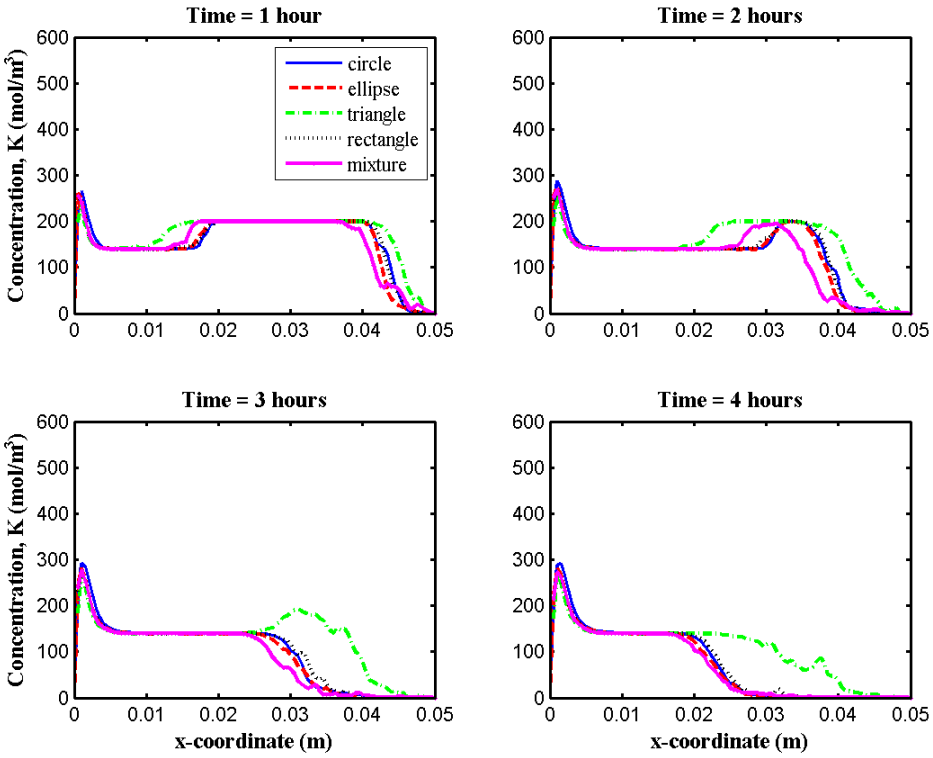

Figure 6. Comparisons of potassium concentration profiles for different aggregate shapes, V_{agg} = 0.5.

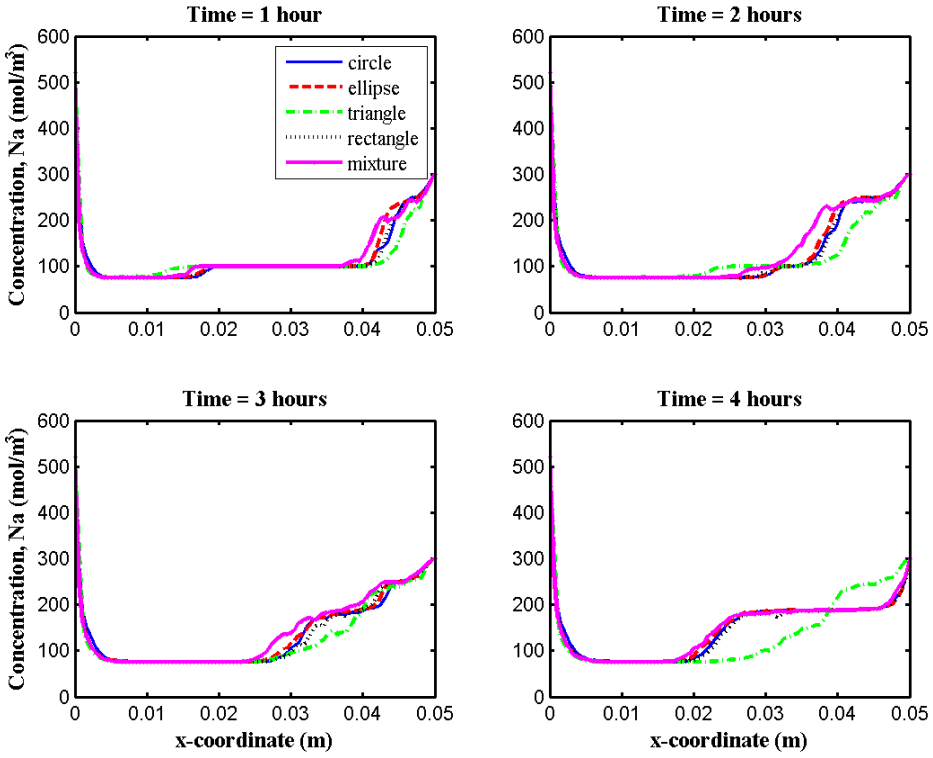

Figure 7. Comparisons of sodium concentration profiles for different aggregate shapes, V_{agg} = 0.5

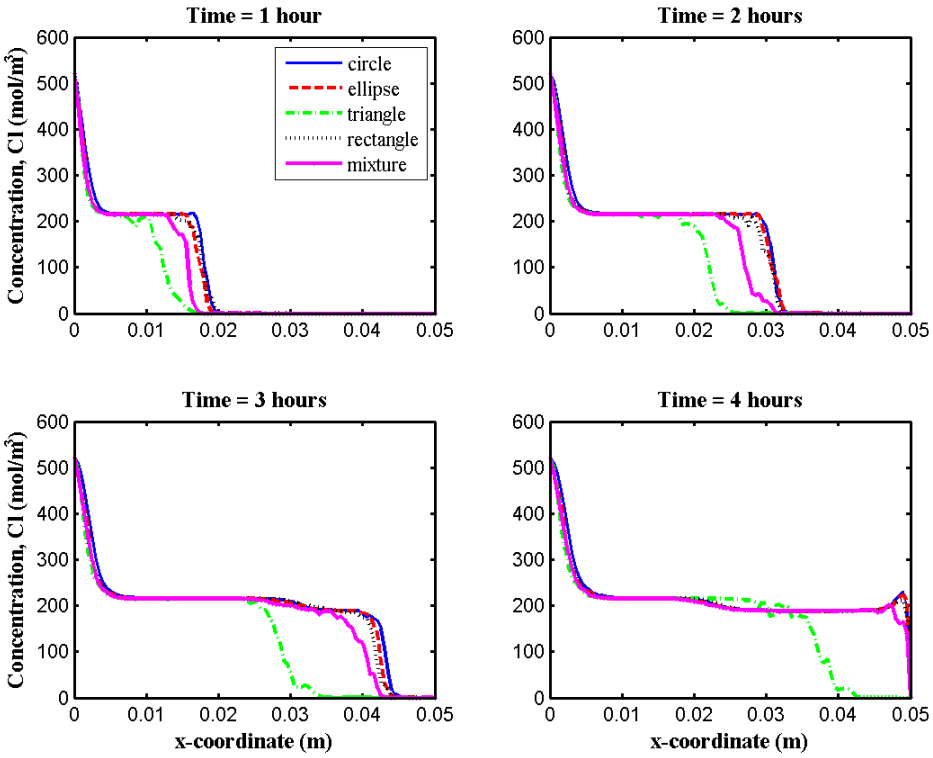

Figure 8. Comparisons of chloride concentration profiles for different aggregate shapes, V_{agg} = 0.5.

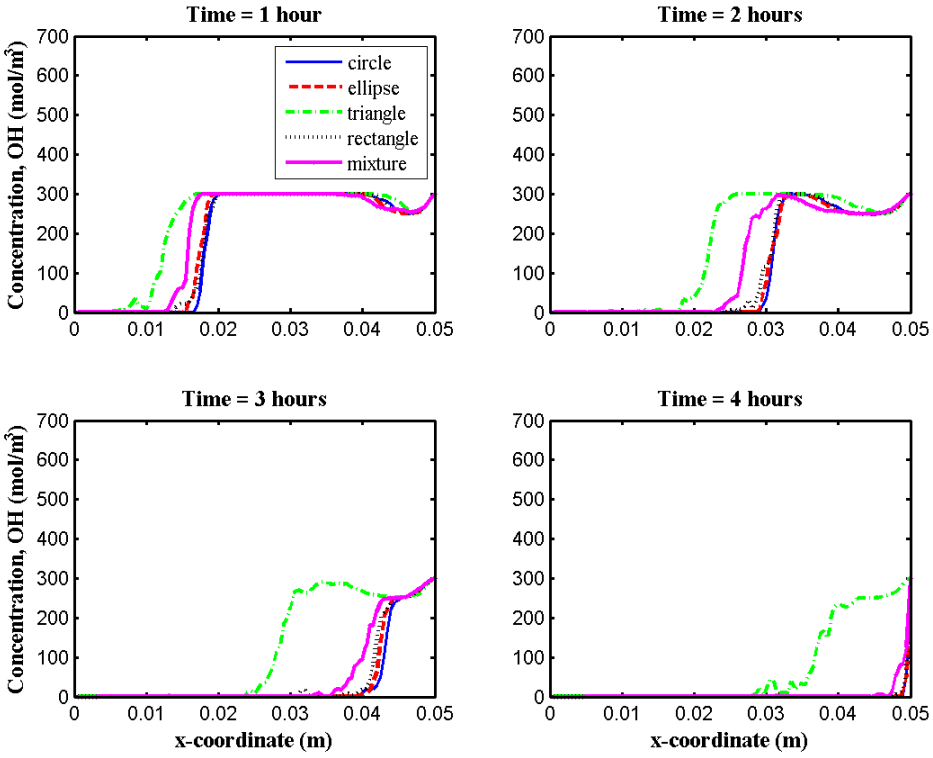

Figure 9. Comparisons of hydroxide concentration profiles for different aggregate shapes, V_{agg} = 0.5.

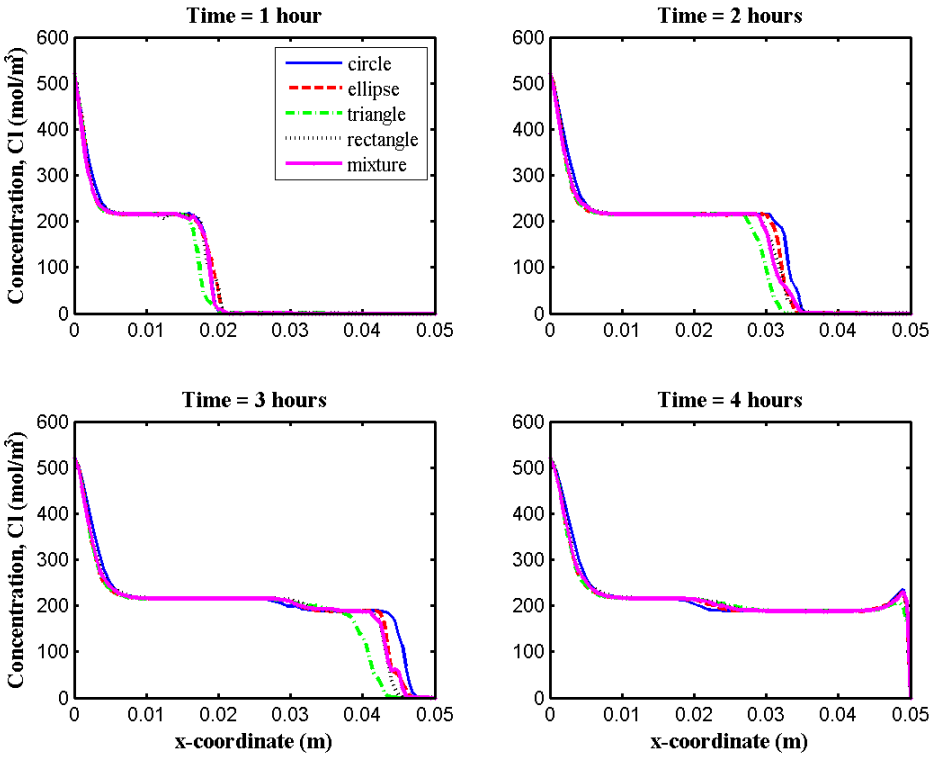

Figure 10. Comparisons of chloride concentration profiles for different aggregate shapes, V_{agg} = 0.3.

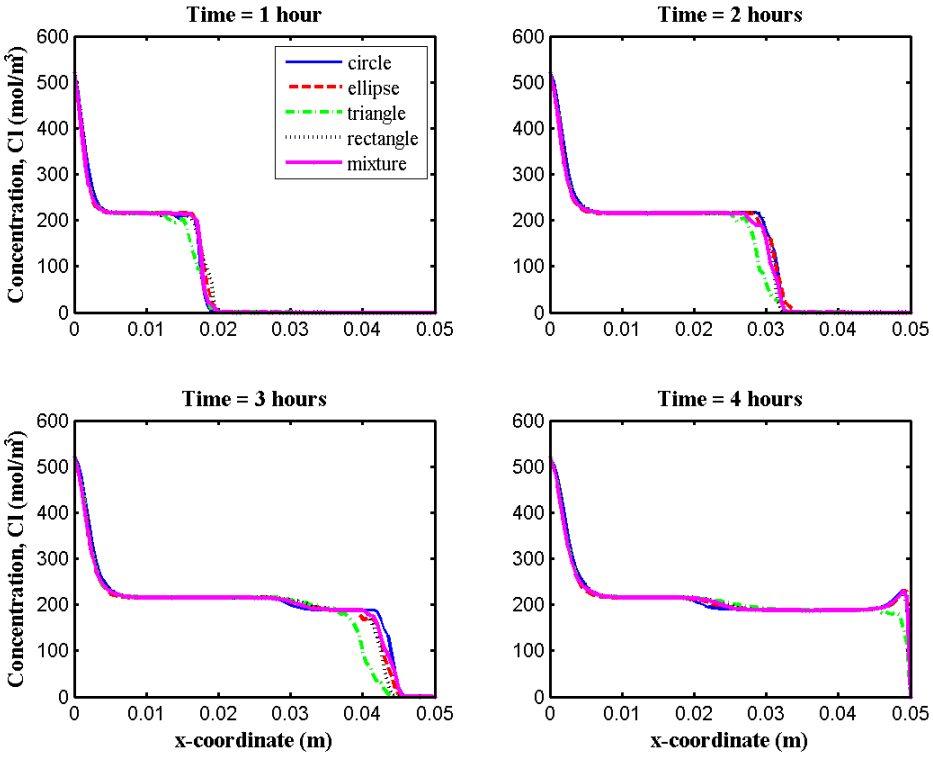

Figure 11. Comparisons of chloride concentration profiles for different aggregate shapes, V_{agg} = 0.4.

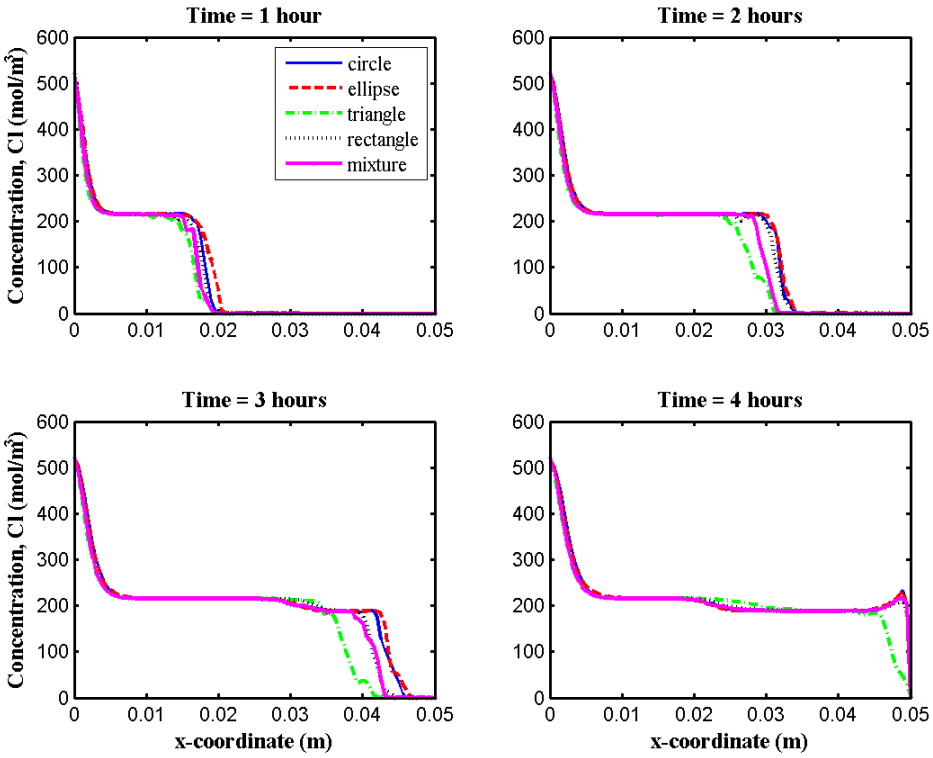

Figure 12. Comparisons of chloride concentration profiles for different aggregate shapes, V_{agg} = 0.45.

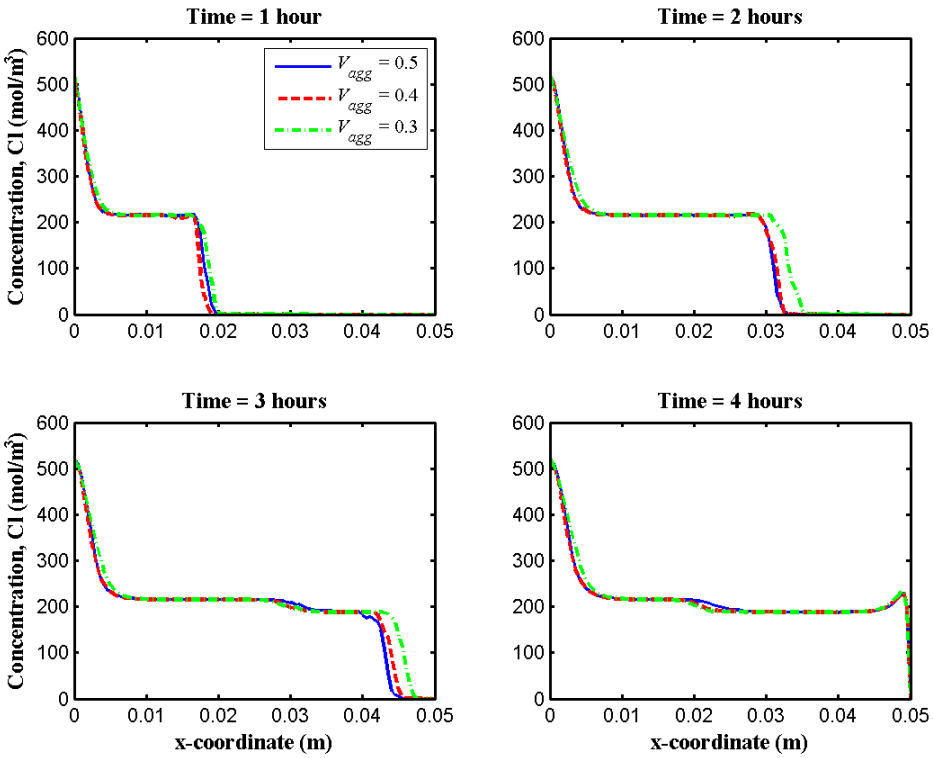

Figure 13. Comparisons of chloride concentration profiles for different volume fractions (circular aggregates)